

# Leading twist nuclear shadowing and suppression of hard coherent diffraction in proton-nucleus scattering

V. Guzey

*Institut für Theoretische Physik II,  
Ruhr-Universität Bochum, D-44780 Bochum, Germany\**

M. Strikman

*Department of Physics, Pennsylvania State University, University Park, PA 16802, USA†*

## Abstract

We use the Glauber-Gribov multiple scattering formalism and the theory of leading twist nuclear shadowing to develop a method for the calculation of leading twist hard coherent diffraction in hadron-nucleus processes. We demonstrate that soft multiple rescatterings lead to the factorization breaking of hard diffraction in proton-nucleus scattering, which is larger than in hadron-nucleon scattering. At the LHC and RHIC kinematics, we compare the hard diffractive to e.m. mechanisms of hard coherent production of two jets in proton-nucleus scattering. We study the  $x_{\mathbb{P}}$ ,  $\beta$  and  $A$ -dependence of the ratio of the dijet production cross sections due to the two effects,  $R$ . We demonstrate that in proton-heavy nucleus hard coherent diffraction at the LHC,  $R$  is small, which offers a clean method to study hard photon-proton scattering at the energies exceeding the HERA energies by the factor of ten. On the other hand, the use of lighter nuclei, such as  $^{40}\text{Ca}$ , will allow to study the screened nuclear diffractive parton distribution. Moreover, a comparison of the dijet diffractive production to the heavy-quark-jet diffractive production will estimate the screened nuclear diffractive gluon PDF, which will be measured in nucleus-nucleus ultraperipheral collisions at the LHC.

PACS numbers: 24.85.+p, 25.40.Ep, 13.87.-a

---

\*vadim.guzey@tp2.ruhr-uni-bochum.de

†strikmman@phys.psu.edu

## I. INTRODUCTION

In hadron-hadron scattering at high energies, diffractive processes are characterized by the rapid  $t$ -dependence and by the absence of detected particles in a certain region of the final phase space or, in other words, by the presence of the rapidity gap. When a hard scale is present in diffractive scattering, such processes are called hard diffractive. The phenomenon of hard diffraction in proton-antiproton scattering was first discovered in the  $p\bar{p} \rightarrow pX$  reaction at the the SPC collider at CERN, when it was observed that the diffractive final state  $X$  with the invariant mass in the range 105 to 190 GeV contained jets with the transverse energy between 5 and 13 GeV (the hard scale is given by the jet transverse momentum) [1]. Later, hard diffraction in proton-antiproton scattering was studied at the Tevatron in dijet,  $W$ ,  $b$ -quark and  $J/\Psi$  production, see [2] for a review. The cross section of each hard diffractive channel constitutes approximately 1% of the contribution of the corresponding channel to the inclusive  $p\bar{p}$  cross section.

Turning to electron-proton deep inelastic scattering (DIS), it was one of HERA surprises to observe that hard diffractive events characterized by a large rapidity gap between the virtual photon and the proton fragmentation regions constitute about 10% of the total rate of events [3]. In DIS, the hard scale is provided by the virtuality of the photon,  $Q^2$ .

In the theoretical treatment of soft diffractive processes, the key role is played by the concept of the "Pomeron", the Regge trajectory with vacuum quantum numbers, which provides the diffractive exchange and determines the high-energy behavior of elastic and diffractive scattering amplitudes. In the context of hard diffraction, the notion of Pomeron appears as follows. The QCD factorization theorem for hard diffraction in DIS [4] enables one to introduce universal diffractive parton distribution functions (PDFs), which can relate such processes as inclusive diffraction, dijet diffractive production,  $D^*$ -meson diffractive production, etc. Making an assumption that the diffractive PDFs can be factorized into the product of two terms, representing the Pomeron flux and the Pomeron parton distributions, one can effectively study the parton content of the Pomeron, similarly to the parton content of the nucleon in inclusive DIS [5, 6, 7, 8, 9].

A comparison of hard diffraction in proton-antiproton scattering at the Tevatron to hard diffraction in electron-proton scattering at HERA indicates the breakdown of the QCD factorization: The use of diffractive PDFs extracted from the HERA measurements significantly

overestimates the rates of hard diffraction at the Tevatron [2, 10]. This can be explained by the absorptive effects associated with multi-Pomeron exchanges, which make the gap survival very unlikely in the case of hadronic collisions [11], or by the gradual onset of the so-called black disk regime for the proton-proton collisions at small impact parameters [12].

Turning to diffraction in hadron-nucleus and lepton-nucleus scattering, the situation can be briefly summarized as follows. Soft coherent (without the nuclear break-up) diffraction in hadron-nucleus scattering at high energies can be successfully described within the framework of the Glauber-Gribov approach by taking into account cross section (color) fluctuations in the hadronic projectile [13, 14, 15, 16], see also Sect. II.

In DIS on nuclear targets, nuclear diffractive PDFs at small values of Bjorken  $x$  can be expressed in terms of the nucleon diffractive PDFs, which are known from the HERA studies [17]. This approach to nuclear diffractive PDFs and to usual nuclear parton distribution functions is based on the Gribov's connection between the nuclear shadowing correction and the elementary diffractive cross section, the QCD factorization theorem for hard diffraction in DIS [4] and the QCD analysis of HERA data on hard diffraction [5, 6, 7, 8, 9], see [18] and references therein and also Sect. II.

In this work, we study hard diffraction in proton-nucleus collisions. As an example, we derive the expression for the cross section of the hard coherent diffractive production of two jets in proton-nucleus scattering. We analyze the suppression of hard diffraction in proton-nucleus scattering compared to hard diffraction in proton-proton scattering. A numerical analysis of the corresponding suppression factor enables us to quantify the QCD factorization breaking in hard proton-nucleus diffraction due to the soft screening (absorption).

The paper consists of two parts. In Sect. II, we derive a general expression for the nuclear modifications of hard diffraction in proton-nucleus scattering. We demonstrate that because of multiple soft rescatterings, hard diffractive processes such as production of two jets, heavy flavors, etc. are suppressed at the LHC and RHIC energies stronger than soft inelastic diffraction, which in turn is expected to be strongly suppressed [13, 15, 16].

In Sect. III, we compare the contribution of hard coherent proton-nucleus diffraction into two jets (including heavy-quark jets) to the e.m. contribution, when the final state containing two hard jets is produced by the coherent nuclear Coulomb field. We demonstrate that the e.m. contribution dominates proton-heavy nucleus (such as  $^{208}\text{Pb}$ ) scattering at the LHC, which provides essentially a background-free method to study very high-energy  $\gamma p$  scattering

at the LHC through ultraperipheral proton-nucleus scattering. We show that using lighter nuclei, which do not produce such a strong flux of equivalent photons as  $^{208}\text{Pb}$ , one can study screened nuclear diffractive PDFs. In this case, a comparison of the dijet diffractive production to the heavy-quark-jet diffractive production will measure the nuclear screened diffractive gluon PDF. The latter can be compared to the nuclear diffractive PDFs, which will be measured in nucleus-nucleus ultraperipheral collisions at the LHC. The conclusion about the dominance of the hard diffractive mechanism over the e.m. one, when light nuclei are used, also holds in the RHIC kinematics.

Our results are also valid for the diffraction in resolved photon-nucleus interactions. Since in this case several other effects are also important, we will discuss hard diffraction in  $\gamma A$  interactions in a separate publication.

## II. SUPPRESSION FACTOR FOR HARD PROTON-NUCLEUS DIFFRACTION

The derivation of the expression for the amplitude of hard diffraction in hadron-nucleus scattering combines features of soft coherent diffraction in hadron-nucleus scattering and hard coherent diffraction in DIS on nuclear targets. Therefore, we shall briefly review coherent soft and hard diffraction below.

### A. Soft coherent proton-nucleus diffraction

At high energies, the cross section of soft coherent hadron-nucleus diffraction (diffraction dissociation),  $\sigma_{DD}^{hA}$ , can be economically and reliably calculated using the Glauber-Gribov multiple scattering formalism [19, 20, 21] generalized to include the so-called cross section (color) fluctuations in the projectile [13, 14, 15, 16]

$$\sigma_{DD}^{hA} = \int d^2b \left( \int d\sigma P(\sigma) |\Gamma_A(b, \sigma)|^2 - \left| \int d\sigma P(\sigma) \Gamma_A(b, \sigma) \right|^2 \right). \quad (1)$$

In Eq. (1),  $b$  is the impact parameter (the two-dimensional vector connecting the trajectory of the projectile with the center of the target nucleus);  $P(\sigma)$  is the probability to find in the projectile a hadronic configuration, which interacts with target nucleons with the cross section  $\sigma$ ;  $\Gamma_A$  is the projectile-nucleus scattering amplitude in the impact parameter

space [20]

$$\Gamma_A(b, \sigma) = 1 - \exp\left(-\frac{1}{2}\sigma T_A(b)\right), \quad (2)$$

where  $T_A(b) = \int dz \rho_A(b, z)$  and  $\rho_A$  is the nucleon density normalized to the number of the nucleons  $A$ . The energy-dependence of  $\sigma_{DD}^{hA}$  is determined by the energy-dependence of  $P(\sigma)$ , which is implied [16]. Note that in Eq. (2), we neglected the slope of the elementary hadron-nucleon scattering amplitude compared to the nuclear size and we assumed that the elementary scattering amplitude is purely imaginary, which is a good approximation at the high energies that we consider in this work.

The function  $P(\sigma)$  describes the probability that the incoming hadron interacts with target nucleons with a given cross section  $\sigma$ . In other words,  $P(\sigma)$  describes cross section fluctuations in the energetic projectile. The notion of  $P(\sigma)$  is introduced in order to have a compact phenomenological description of soft coherent diffraction in hadron-nucleon and hadron-nucleus scattering. As follows from Eq. (1), ignoring cross section fluctuation, i.e. setting  $P(\sigma) \propto \delta(\sigma - \sigma_{\text{tot}})$ , would result in the unacceptable result that  $\sigma_{DD}^{hA} = 0$ .

The formalism of cross section fluctuations is based on the simple picture of diffractive dissociation in the laboratory reference frame developed by Feinberg and Pomeranchuk [22] and by Good and Walker [23]. In this picture, the incoming hadron is represented by a coherent superposition of eigenstates of the scattering operator. Since different eigenstates correspond to different  $\sigma$ , the scattered state is in general different from the incoming state, but it has the same quantum numbers. This corresponds to the process of diffractive dissociation.

One should note that the formalism of cross section fluctuations implicitly uses the assumption of the completeness of the scattering eigenstates and, hence, it is applicable only at  $t \approx 0$ . At  $t \neq 0$ , the diffractive final state can be produced as a result of some effective interaction or as a result of hard parton scattering (for sufficiently large  $t$ ), which have nothing to do with the cross section fluctuations in the projectile.

The function  $P(\sigma)$  is different for different projectiles (protons, pions, photons). For the proton,  $P(\sigma)$  has a narrow dispersion around  $\sigma = \sigma_{\text{tot}}$ , where  $\sigma_{\text{tot}}$  is the total proton-nucleon cross section. Therefore, one can Taylor-expand the integrand in Eq. (1) around  $\sigma_{\text{tot}}$  and keep only first two non-vanishing terms

$$\sigma_{DD}^{hA} \approx \frac{\omega_\sigma \sigma_{\text{tot}}^2}{4} \int d^2b T_A^2(b) e^{-\sigma_{\text{tot}} T_A(b)}. \quad (3)$$

In Eq. (3),  $\omega_\sigma$  is the energy-dependent parameter, which is proportional to the proton-proton diffractive dissociation cross section and which controls the magnitude of cross section fluctuations

$$\omega_\sigma = \frac{\int d\sigma \sigma^2 P(\sigma)}{[\int d\sigma \sigma P(\sigma)]^2} - 1. \quad (4)$$

Equation (1) can be interpreted as follows. The incoming proton diffractively dissociates on the front face of the target nucleus. The corresponding scattering amplitude squared is proportional to  $\omega_\sigma \sigma_{\text{tot}}^2 T_A^2(b)$ . On the way through the nucleus, the produced diffractive state interacts with all nucleons of the target and becomes partially absorbed (suppressed). The corresponding soft suppression factor can be read off from Eq. (3),

$$T_{\text{soft}}^{pA} = \exp(-\sigma_{\text{tot}} T_A(b)). \quad (5)$$

Note that since we have assumed that the dispersion of  $P(\sigma)$  around  $\sigma = \sigma_{\text{tot}}$  is small, the soft suppression factor depends only on  $\sigma_{\text{tot}}$ .

## B. Hard coherent diffraction in DIS on nuclear targets

Inclusive and coherent DIS on nuclear targets measure usual and diffractive nuclear parton distribution functions (PDFs), respectively. The theory of leading twist nuclear shadowing of usual and diffractive nuclear PDFs is based on the Gribov's relation between nuclear shadowing and diffraction [21, 24], Collins' factorization theorem for hard diffraction in DIS [4] and the QCD analysis of the HERA data on hard diffraction in DIS on hydrogen [5, 6, 7, 8, 9], see [18] for the review and references.

According to this approach, the nuclear shadowing correction,  $\delta f_{j/A}$ , to the nuclear PDF of the flavor  $j$ ,  $f_{j/A} = Af_{j/N} - \delta f_{j/A}$ , is expressed in terms of the proton diffractive PDF  $f_{j/N}^{D(4)}$  [17, 24]

$$\begin{aligned} \delta x f_{j/A}(x, Q_0^2) &= 8\pi \Re e \left[ \frac{(1-i\eta)^2}{1+\eta^2} \int d^2b \int_{-\infty}^{\infty} dz_1 \int_{z_1}^{\infty} dz_2 \int_x^{x_0} dx_{\mathbb{P}} \beta f_{j/N}^{D(4)}(x, Q_0^2, x_{\mathbb{P}}, t=0) \right. \\ &\quad \left. \times \rho_A(b, z_1) \rho_A(b, z_2) e^{ix_{\mathbb{P}} m_N (z_1 - z_2)} e^{-\frac{1-i\eta}{2} \sigma_{\text{eff}}^j(x, Q_0^2) \int_{z_1}^{z_2} dz' \rho_A(b, z')} \right]. \quad (6) \end{aligned}$$

In Eq. (6),  $x$  and  $Q_0^2$  are the Bjorken variables;  $x_{\mathbb{P}}$  is the target longitudinal momentum fraction loss or the longitudinal momentum fraction carried by the diffractive exchange

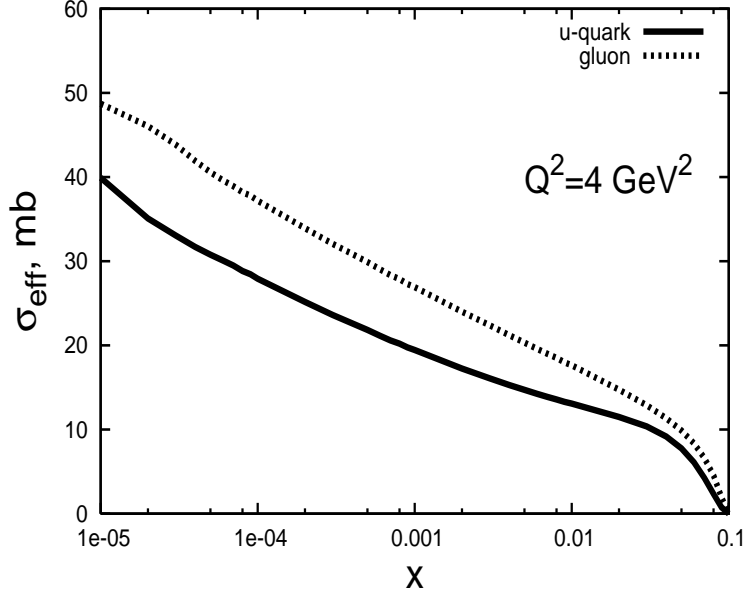


FIG. 1: The effective cross section  $\sigma_{\text{eff}}^j$  of Eq. (7) for  $\bar{u}$ -quarks and gluons at  $Q_0^2 = 4 \text{ GeV}^2$ .

(the "Pomeron");  $\beta = x/x_{\mathcal{P}}$ ;  $x_0 = 0.1$ ;  $\sigma_{\text{eff}}^j$  is the effective rescattering cross section of the intermediate diffractive state;  $\eta$  is the ratio of the real to the imaginary parts of the elementary diffractive amplitude. In the present analysis,  $\eta = \pi/2 (\alpha_{\mathcal{P}}(0) - 1) = 0.185$  [8, 9].

It is important to mention that since the  $t$ -dependence of the nuclear form factor is much steeper than that of the nucleon diffractive structure function, it is a good approximation to use  $f_{j/N}^{D(4)}(x, Q_0^2, x_{\mathcal{P}}, t_{\text{min}})$  [ $t_{\text{min}} \approx -(x_{\mathcal{P}} m_N)^2$ ] instead of  $f_{j/N}^{D(4)}(x, Q_0^2, x_{\mathcal{P}}, t)$  in Eq. (6). Moreover, in the considered range of Bjorken  $x$ ,  $t_{\text{min}}$  is small enough so that  $f_{j/N}^{D(4)}(x, Q_0^2, x_{\mathcal{P}}, t_{\text{min}})$  and  $f_{j/N}^{D(4)}(x, Q_0^2, x_{\mathcal{P}}, t = 0)$  practically coincide.

As follows from Eq. (6),  $\sigma_{\text{eff}}^j$  determines the nuclear correction to  $\delta f_{j/A}$  due to the interaction with two and more nucleons (the interaction associated with the rescattering of the intermediate diffractive state). This cross section is defined in terms of the nucleon diffractive ( $f_{j/N}^{D(4)}$ ) and usual ( $f_{j/N}$ ) PDFs [18, 24]

$$\sigma_{\text{eff}}^j(x, Q_0^2) = \frac{16\pi}{x f_{j/N}(x, Q_0^2)} \int_x^{x_0} dx_{\mathcal{P}} \beta f_{j/N}^{D(4)}(\beta, Q_0^2, x_{\mathcal{P}}, t = 0). \quad (7)$$

Figure 1 presents  $\sigma_{\text{eff}}^j$  for gluons and  $\bar{u}$ -quarks as a function of  $x$  at  $Q_0^2 = 4 \text{ GeV}^2$ . We used the recent QCD analysis of H1 data on hard diffraction at HERA [8, 9] and CTEQ5M fit to inclusive PDFs [25].

Also, since Eq. (7) involves the nucleon diffractive PDFs at  $t = 0$ , one has to make

an assumption about the  $t$ -dependence of the nucleon diffractive PDFs. Experimentally, the  $t$ -dependence of the diffractive cross section is found to be practically constant as a function of  $\beta$ , while the contribution of the gluon diffractive PDF increases strongly with a decrease of  $\beta$  [8, 9]. Hence, in this work, we assume that all PDFs have the same exponential  $t$ -dependence,

$$f_{j/N}^{D(4)}(\beta, Q_0^2, x_P, t) = e^{-B_{\text{diff}}|t|} f_{j/N}^{D(4)}(\beta, Q_0^2, x_P, t = 0), \quad (8)$$

where  $B_{\text{diff}} = 6 \text{ GeV}^{-2}$  is taken from the recent H1 measurement with the leading proton spectrometer [9].

Figure 2 presents an example of our calculation of nuclear shadowing for nuclear PDFs of  $^{40}\text{Ca}$  and  $^{208}\text{Pb}$  as a function of  $Q^2$  and Bjorken  $x$ . The solid curve corresponds to the ratio  $f_{j/A}/(Af_{j/N})$  for  $\bar{u}$ -quarks; the dotted curve corresponds to gluons. The lower set of curves corresponds to  $Q^2 = Q_0^2 = 4 \text{ GeV}^2$ . In addition to nuclear shadowing given by Eq. (6), we have introduced an enhancement (antishadowing) of nuclear gluon PDF on the interval  $0.03 \leq x \leq 0.2$ , which is modelled by requiring the conservation of the momentum sum rule, see e.g. [18]. The two other sets of predictions for  $Q^2 = 10 \text{ GeV}^2$  and  $Q^2 = 100 \text{ GeV}^2$  are obtained by NLO DGLAP evolution.

We would like to point out that the numerical analysis of nuclear shadowing presented in this work differs from our earlier analyses, see e.g. [18], because we now use the most recent H1 fits to nuclear diffractive PDFs and a different value of  $B_{\text{diff}}$ , see Eq. (8). However, the changes in the predicted nuclear shadowing are not large. The ratio  $f_{j/A}/(Af_{j/N})$  for  $\bar{u}$ -quarks in Fig. 2 is very similar to our earlier result [18]. In the gluon channel, the ratio  $f_{j/A}/(Af_{j/N})$  in Fig. 2 is similar to the lower-gluon-shadowing scenario of [18].

Next we turn to nuclear diffractive PDF. In the Glauber-Gribov approach, the nuclear diffractive PDF of the flavor  $j$ ,  $f_{j/A}^{D(3)}$ , is expressed in terms of the proton diffractive PDF  $f_{j/N}^{D(4)}$  as follows [17]

$$\begin{aligned} x f_{j/A}^{D(3)}(x, Q_0^2, x_P) &= 4 \pi \beta f_{j/N}^{D(4)}(x, Q_0^2, x_P, t = 0) \int d^2b \\ &\times \left| \int_{-\infty}^{\infty} dz e^{ix_P m_N z} e^{-\sigma_{\text{eff}}^j(x, Q_0^2)/2} \int_z^{\infty} dz' \rho_A(b, z') \rho_A(b, z) \right|^2 \\ &\approx 16 \pi f_{j/N}^{D(4)}(x, Q_0^2, x_P, t = 0) \int d^2b \left( \frac{1 - e^{-\sigma_{\text{eff}}^j(x, Q_0^2)/2 T_A(b)}}{\sigma_{\text{eff}}^j(x, Q_0^2)} \right)^2. \quad (9) \end{aligned}$$

The last line is an approximation valid at small  $x_P$ , when the effect of the coherence length



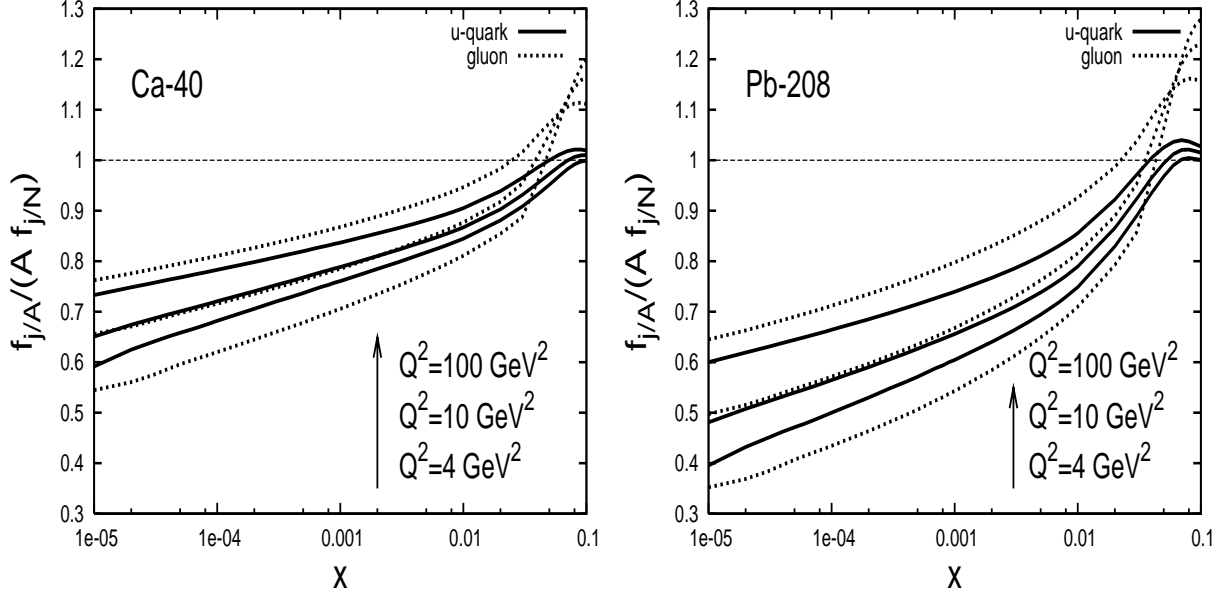


FIG. 2: The ratio of the nuclear to nucleon PDFs,  $f_{j/A}/(A f_{j/N})$ , for  $^{40}\text{Ca}$  and  $^{208}\text{Pb}$  at  $Q^2 = 4, 10$  and  $100 \text{ GeV}^2$  as a function of Bjorken  $x$ , see Eq. (6). The solid curve corresponds to  $\bar{u}$ -quarks; the dotted curve corresponds to gluons.

[the factor  $\exp(ix_{\mathcal{P}}m_N z)$ ] can be neglected. In the opposite limit of large  $x_{\mathcal{P}}$ ,  $x_{\mathcal{P}} \geq 0.05$ , the dominant contribution to the nuclear diffractive structure function is given by the impulse approximation, i.e. by Eq. (9) where  $\sigma_{\text{eff}}^j$  is set to zero. In Eq. (9), the superscripts (3) and (4) denote the dependence on three and four variables, respectively. Note that similarly to Eq. (3), we neglected the slope and the real part of the elementary diffractive amplitude in Eq. (9).

One can quantify nuclear diffractive PDFs by introducing the probability of diffraction for a given parton flavor  $j$ ,  $P_{\text{diff}}^j$  [24],

$$P_{\text{diff}}^j = \frac{\int_x^{x_0} dx_{\mathcal{P}} x f_j^{D(3)}(x, Q_0^2, x_{\mathcal{P}})}{x f_j(x, Q_0^2)}. \quad (10)$$

An example of the evaluation of the probability of hard diffraction in DIS according to Eq. (10) is presented in Fig. 3, where  $P_{\text{diff}}^j$  is plotted at fixed  $Q_0^2 = 4 \text{ GeV}^2$  as a function of Bjorken  $x$ . The left panel corresponds to DIS on  $^{40}\text{Ca}$ ; the right panel corresponds to DIS on  $^{208}\text{Pb}$ . For comparison, the results for DIS on hydrogen are also given by thin curves. The solid curves correspond to the  $\bar{u}$ -quark channel; the dotted curves correspond to the gluon channel.

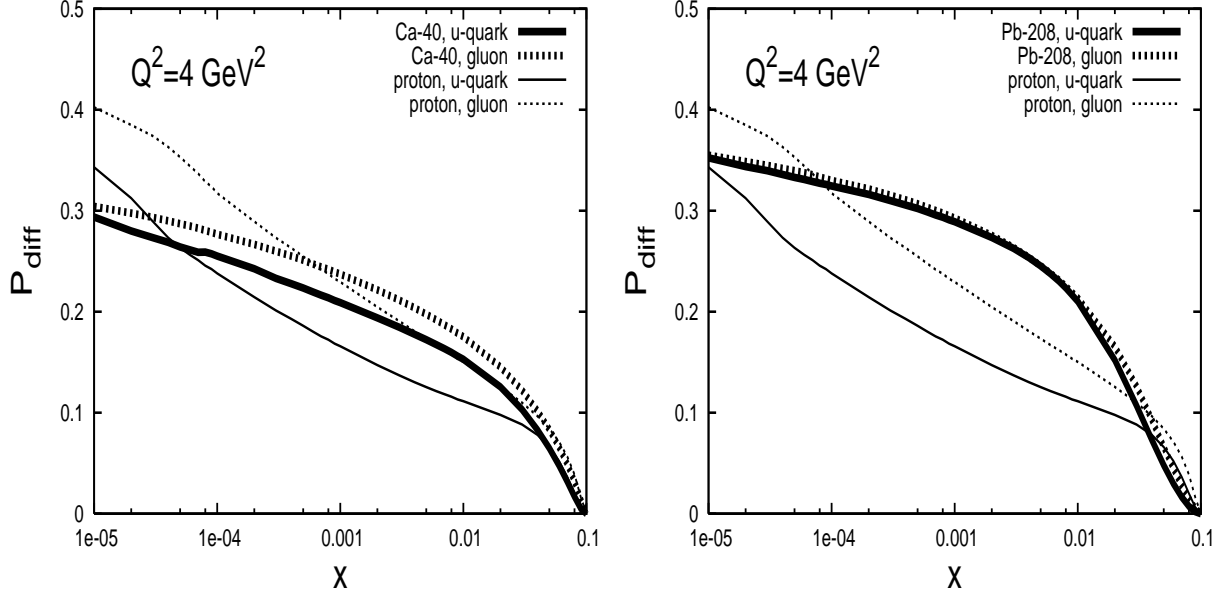


FIG. 3: The probability of hard diffraction in DIS,  $P_{\text{diff}}^j$ , see Eq. (10). The left panel corresponds to DIS on  $^{40}\text{Ca}$ ; the right panel corresponds to DIS on  $^{208}\text{Pb}$ . For comparison, the results for DIS on hydrogen are given by thin curves. The solid curves correspond to the  $\bar{u}$ -quark channel; the dotted curves correspond to the gluon channel.

We would like to point out the following two features of  $P_{\text{diff}}^j$  presented in Fig. 3. First, the difference between the quark and the gluon channels is very small. While the quark and gluon diffractive and usual nuclear PDFs are different, their difference cancels to a large extent in the ratio  $P_{\text{diff}}^j$  (the cancellation is larger for heavier nuclei). Second, even for such a heavy nucleus as  $^{208}\text{Pb}$ ,  $P_{\text{diff}}^j \leq 0.36$ , which should be compared to the asymptotic ( $A \rightarrow \infty$  and  $\sigma_{\text{eff}}^j \rightarrow \infty$ ) upper limit  $P_{\text{diff}}^j = 0.5$ . An examination shows that while close to the center of the nucleus ( $b \approx 0$ ), the probability of diffraction is very close to  $1/2$ , the contribution of the nuclear edge significantly dilutes  $P_{\text{diff}}^j$ .

Equation (9) can be interpreted as follows. The incoming virtual photon fluctuates into its hard diffractive component long time before the photon interacts with the target (we ignore the effect of the finite coherent length). The hard diffractive component elastically rescatters on the target nucleus, which gives the suppression factor  $[1 - \exp(-\frac{1}{2}\sigma_{\text{eff}}^j(x, Q_0^2) T_A(b))]^2$ , and emerges as the final hard diffractive state.

One should note that the approximate expression for  $f_{j/A}^{D(3)}$  [the last line in Eq. (9)]

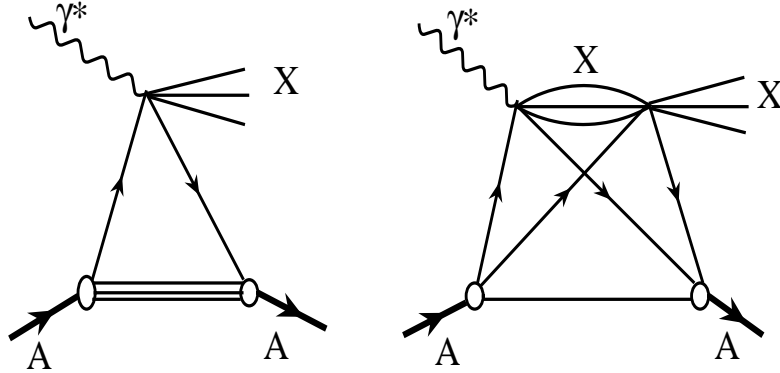


FIG. 4: Feynman graphs representing the first two terms of the multiple scattering series (9) for the nuclear diffractive parton distribution  $f_{j/A}^{D(3)}$ .

corresponds to the first term in Eq. (3) since the elastic contribution to DIS is absent (suppressed by the smallness of  $\alpha_{e.m.}$ ). Therefore, the analogy between Eqs. (3) and (9) enables us to introduce the attenuation factor characterizing the suppression of hard coherent diffraction in DIS on nuclear targets due to nuclear shadowing,

$$T_{\text{hard}}^{\gamma^*A} = \exp(-\sigma_{\text{eff}}^j(x, Q_0^2) T_A(b)) . \quad (11)$$

The graphical representation of Eq. (9), when only the interaction with one and two nucleons of the target is retained, is shown in Fig. 4. The right graph helps to understand why  $T_{\text{hard}}^{\gamma^*A}$  is driven by  $\sigma_{\text{eff}}^j$ . As seen from the graph, the strength of the hard rescattering is defined by the  $XN \rightarrow XN$  cross section summed over all  $X$ . This cross section is nothing but the ratio of the  $\gamma^*N \rightarrow XN$  to the  $\gamma^*N \rightarrow X$  cross sections summed over  $X$ , which corresponds exactly to  $\sigma_{\text{eff}}^j$  defined by Eq. (7).

It is important to emphasize that, in general, the calculation of  $T_{\text{hard}}^{\gamma^*A}$  is model-independent only for the interaction with one or two nucleons. For the interaction with  $N \geq 3$  nucleons, we implicitly used the so-called quasi-eikonal approximation in Eq. (11), which assumes that the diffractively produced state elastically rescatters on the nucleons. This approximation is equivalent to the observation of the small dispersion of  $P(\sigma)$  used in the derivation of Eq. (3).

### C. Hard coherent proton-nucleus diffraction

As an example of hard coherent diffractive processes on heavy nuclear targets, we consider the hard coherent diffractive production of two jets in the reaction  $p + A \rightarrow 2 \text{ jets} + X + A$ . In this process,  $A$  denotes the nucleus;  $X$  denotes the soft diffractive component; the invariant mass of the jets provides the hard scale.

The cross section of the  $p + A \rightarrow 2 \text{ jets} + X + A$  reaction can be readily obtained by generalizing the well-known expression for the dijet inclusive cross section in hadron-hadron scattering [26] and by introducing the new quantity, the screened nuclear diffractive PDFs  $\tilde{f}_{j/A}^{D(3)}$ ,

$$\begin{aligned} & \frac{d^3 \sigma^{p+A \rightarrow 2 \text{ jets} + X + A}}{dx_1 dp_T^2 dx_P} \\ & \propto \sum_{\substack{i,j, \\ k,l=q,\bar{q},g}} f_{i/p}(x_1, Q_{\text{eff}}^2) \tilde{f}_{j/A}^{D(3)}(x_2, Q_{\text{eff}}^2, x_P) \overline{\sum} |\mathcal{M}(ij \rightarrow kl)|^2 \frac{1}{1 + \delta_{kl}}, \end{aligned} \quad (12)$$

where  $f_{i/p}$  are the usual proton PDFs;  $\overline{\sum} |\mathcal{M}(ij \rightarrow kl)|^2$  are the invariant matrix elements for two-to-two parton scattering given in Table 7.1 of [26];  $x_1$  and  $x_2$  are the light-cone momentum fractions of the proton and the nucleus active quarks, respectively;  $p_T$  is the transverse momentum of each of the final jets;  $Q_{\text{eff}}$  is the effective hard scale of the process. For the simplification of our analysis, we consider only the case of  $90^\circ$  hard parton scattering in the center of mass, which constrains  $x_1$  (as a function of  $x_2 = \beta x_P$ ) and  $Q_{\text{eff}}^2$

$$x_1 = \frac{4p_T^2}{\beta x_P s}, \quad Q_{\text{eff}}^2 = 4p_T^2, \quad (13)$$

where  $\sqrt{s}$  is the proton-nucleon invariant energy. The term "screened PDF" means that this parton distribution contains certain soft suppression effects, i.e. the screened PDF is suppressed compared to the analogous PDF extracted from hard processes.

The derivation of the expression for the screened nuclear diffractive PDFs,  $\tilde{f}_{j/A}^{D(3)}$ , is carried out similarly to the derivation of Eq. (3) [see also Fig. 5]

$$\tilde{f}_{j/A}^{D(3)}(x, Q_0^2, x_P) \approx 4\pi \tilde{f}_{j/N}^{D(4)}(x, Q_0^2, x_P, t=0) \int d^2b T_A^2(b) e^{-(\sigma_{\text{tot}}(s) + \sigma_{\text{eff}}^j(x, Q_0^2))T_A(b)}, \quad (14)$$

where  $\tilde{f}_{j/N}^{D(4)}$  is the screened diffractive PDF of the nucleon, which enters the QCD description of the  $p + p \rightarrow 2 \text{ jets} + X + p$  reaction;  $\sigma_{\text{tot}}$  is the total proton-nucleon cross section;  $\sigma_{\text{eff}}^j$  is the effective rescattering cross section of Eq. (7). In Eq. (14), we neglected the slope and

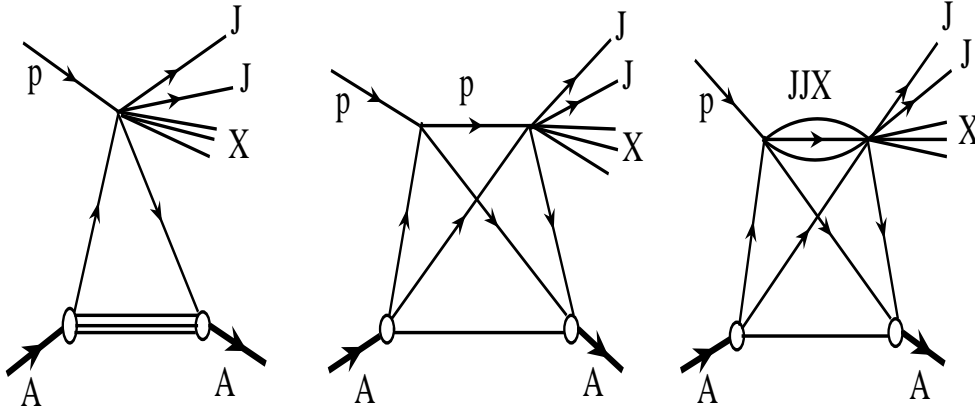


FIG. 5: Feynman graphs representing the first two terms of the multiple scattering series for the  $p + A \rightarrow 2\text{jets} + X + A$  scattering amplitude.

the real part of the elementary  $p + N \rightarrow 2\text{jets} + X + N$  scattering amplitude and a small longitudinal momentum transfer in the  $p + N \rightarrow 2\text{jets} + X + N$  vertex.

It is important to emphasize that in the case of hard coherent proton-nucleus diffraction, the nuclear suppression factor,  $T_{\text{hard}}^{pA}$ , is a product of the soft and hard suppression factors introduced previously,

$$T_{\text{hard}}^{pA} = T_{\text{soft}}^{pA} T_{\text{hard}}^{\gamma^*A}. \quad (15)$$

This can be understood from Fig. 5, which represents the single and double scattering contributions to the  $p + A \rightarrow 2\text{jets} + X + A$  scattering amplitude. The rescattering cross section of the middle graph is  $\sigma_{\text{tot}}$ ; the rescattering cross section of the right graph is  $\sigma_{\text{eff}}^j$  (we assume that all diffractive intermediate states correspond to the same rescattering cross section). Therefore, the resulting nuclear attenuation, which results from the sum of the middle and right graphs, is driven by the  $\sigma_{\text{tot}} + \sigma_{\text{eff}}^j$  cross section.

Equation (14) can be interpreted in two complimentary ways. On the one hand, one can start from soft diffractive dissociation of protons on heavy nuclei, see Eq. (3). Since we are interested in the hard diffractive component of the diffractive dissociation cross section, one has to take into account the additional suppression of nuclear diffractive PDFs given by  $T_{\text{hard}}^{\gamma^*A}$ . As a result, one arrives at Eq. (15). On the other hand, one can start from the expression for inclusive diffraction of protons on nuclei, which is proportional to the

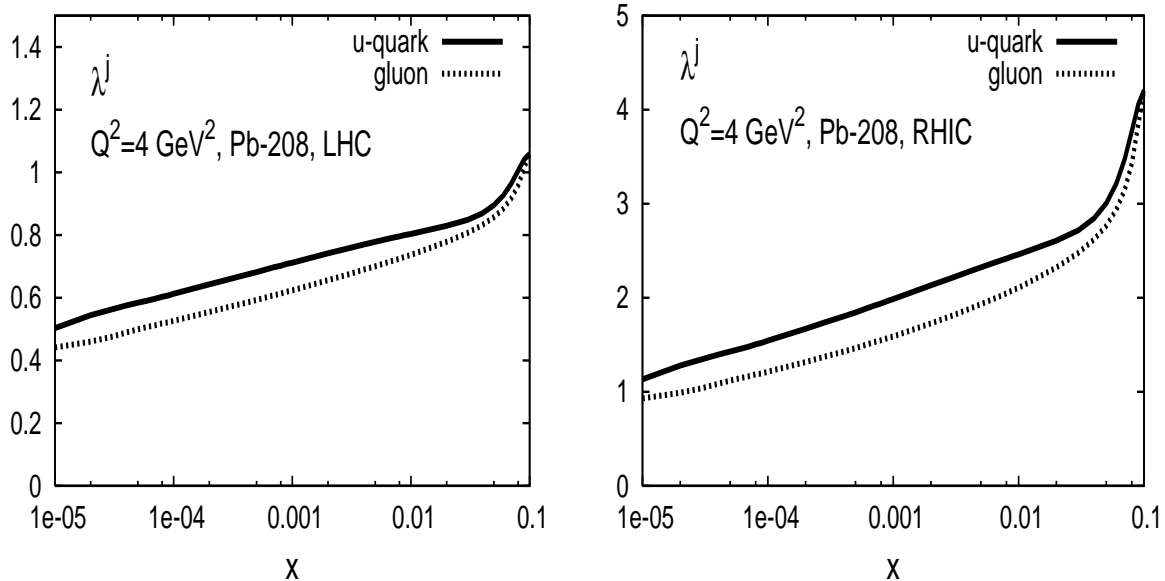


FIG. 6: The suppression factor  $\lambda^j$  of Eq. (16) as a function of Bjorken  $x$  at  $Q^2 = 4 \text{ GeV}^2$  in the LHC ( $\sqrt{s} = 8.8 \text{ TeV}$ ) and RHIC ( $\sqrt{s} = 200 \text{ GeV}$ ) kinematics. The solid curves correspond to the  $\bar{u}$ -quark; the dotted curves correspond to the gluons.

nuclear diffractive PDFs (9). Since the final diffractive state contains a soft component, which is partially absorbed by the nucleus, one should take into account this suppression by introducing the factor  $T_{\text{soft}}^{pA}$ , which represents the probability of the absence of soft inelastic interactions at a given impact parameter  $b$ .

We quantify the suppression of the nuclear screened diffractive PDFs  $\tilde{f}_{j/A}^{D(3)}$  compared to the nucleon screened diffractive PDFs  $\tilde{f}_{j/N}^{D(3)}$  by introducing the factor  $\lambda^j$

$$\begin{aligned} \lambda^j(x, Q^2) &\equiv \frac{\tilde{f}_{j/A}^{D(3)}(\beta, Q^2, x_{\mathcal{P}})}{\tilde{f}_{j/N}^{D(3)}(\beta, Q^2, x_{\mathcal{P}})} = 4\pi \frac{\tilde{f}_{j/N}^{D(4)}(x, Q_0^2, x_{\mathcal{P}}, t=0)}{\tilde{f}_{j/N}^{D(3)}(\beta, Q^2, x_{\mathcal{P}})} \int d^2b T_A^2(b) e^{-(\sigma_{\text{tot}}(s) + \sigma_{\text{eff}}^j(x, Q^2))T_A(b)} \\ &= B_{\text{diff}}(4\pi) \int d^2b T_A^2(b) \exp[-(\sigma_{\text{tot}}(s) + \sigma_{\text{eff}}^j(x, Q^2))T_A(b)], \end{aligned} \quad (16)$$

where in the last line we introduced the slope of the  $t$ -dependence of the screened diffractive PDFs,

$$\tilde{f}_{j/N}^{D(4)}(\beta, Q^2, x_{\mathcal{P}}, t) = \exp(-B_{\text{diff}}|t|) \tilde{f}_{j/N}^{D(4)}(\beta, Q^2, x_{\mathcal{P}}, t=0). \quad (17)$$

Note also that  $\tilde{f}_{j/N}^{D(3)}(\beta, Q^2, x_{\mathcal{P}}) \equiv \int dt \tilde{f}_{j/N}^{D(4)}(\beta, Q^2, x_{\mathcal{P}}, t)$ .

Certain features of Eq. (16) deserve a discussion. First, while the diffractive PDFs depend separately on  $\beta$  and  $x_{\mathcal{P}}$ , the suppression factor  $\lambda^j$  depends only on their product  $x = \beta x_{\mathcal{P}}$

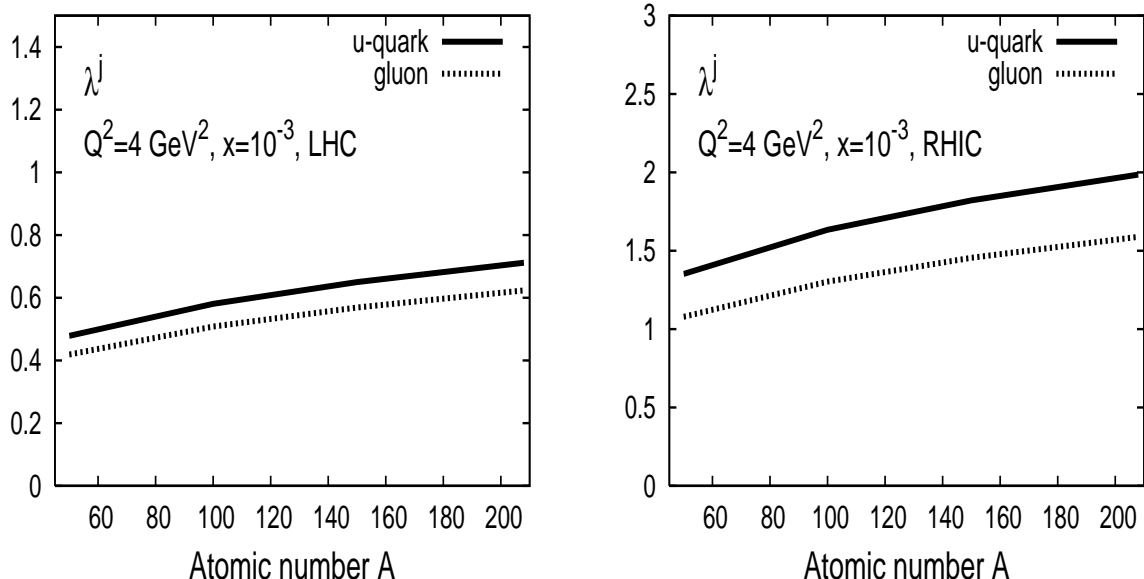


FIG. 7: The suppression factor  $\lambda^j$  of Eq. (16) as a function of the atomic number at  $x = 10^{-3}$  and at  $Q^2 = 4 \text{ GeV}^2$  in the LHC ( $\sqrt{s} \approx 9 \text{ TeV}$ ) and RHIC ( $\sqrt{s} = 200 \text{ GeV}$ ) kinematics. The labeling of the curves is the same as in Fig. 6.

in our approach. Second, at the LHC energies, where  $\sigma_{\text{tot}}$  is of the order of 100 mb, the dependence of  $\lambda^j$  on  $\sigma_{\text{eff}}^j$  is rather weak. Therefore, we expect that  $\lambda^j$  is rather similar for different parton flavors  $j$ . In addition, since the slope  $B_{\text{diff}}$  is independent on the hard scale  $Q^2$  in our approach,  $\lambda^j$  has very weak dependence on  $Q^2$ , which enters only through the  $Q^2$ -dependence of  $\sigma_{\text{eff}}^j$ .

In our numerical analysis of Eq. (16), we used the following input. The slope of the  $t$ -dependence of  $\tilde{f}_{j/N}^{D(4)}$  was taken from the recent H1 measurement of hard inclusive diffraction in DIS on hydrogen,  $B_{\text{diff}} = 6 \text{ GeV}^{-2}$  [9].

The total proton-nucleon scattering cross section,  $\sigma_{\text{tot}}$ , was taken from [27]

$$\sigma_{\text{tot}}(s) = 21.7 s^{0.0808} + 56.08 s^{-0.4525}. \quad (18)$$

The effective cross section  $\sigma_{\text{eff}}^j$  was evaluated using Eq. (7) and the recent QCD fits to the H1 measurement of hard inclusive diffraction on hydrogen [8, 9], see Fig. 1.

For the nucleon density  $\rho_A$ , the two-parameter Fermi model was used [28].

Figures 6 and 7 present the results of our calculations of  $\lambda^j$  in the LHC and RHIC kinematics. The LHC kinematics corresponds to  $\sqrt{s} \approx 9 \text{ TeV}$  per nucleon for proton-

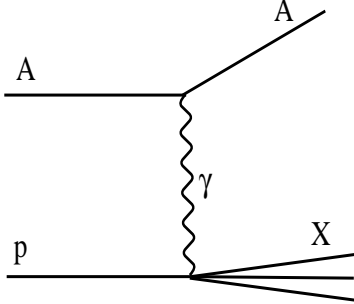


FIG. 8: The ultraperipheral  $p + A \rightarrow X + A$  scattering.

nucleus collisions [29]; the RHIC kinematics corresponds to  $\sqrt{s} = 200$  GeV. Figure 6 gives  $\lambda^j$  as a function of Bjorken  $x$  at  $Q^2 = 4$  GeV<sup>2</sup>. The solid curves correspond to the  $\bar{u}$ -quark; the dotted curves correspond to the gluons. Despite the fact that  $\lambda^j$  is of the order of unity at the LHC and of the order of several units at the RHIC energies, the corresponding suppression of hard diffraction is very large because in the absence of the suppression, nuclear diffractive PDFs are enhanced compared to the nucleon diffractive PDFs by the factor  $f_{j/A}^{D(3)}/f_{j/N}^{D(3)} \propto A^{4/3}$ .

Figure 7 presents the  $A$ -dependence of  $\lambda^j$  at  $x = 10^{-3}$  and at  $Q^2 = 4$  GeV<sup>2</sup>, i.e. at fixed  $\sigma_{\text{eff}}^j$ . As seen from Fig. 7, the  $A$ -dependence of  $\lambda^j$  is rather slow. A simple fit gives that  $\lambda^j \propto A^{0.28}$  at the LHC and RHIC.

### III. HARD DIFFRACTION AND ULTRAPERIPHERAL PROTON-NUCLEUS COLLISIONS

In proton-heavy nucleus ( $^{208}\text{Pb}$ , for example) collisions, most of the diffractive events ( $\sim 80\%$ ) will be generated by the scattering of the proton off the coherent nuclear Coulomb field at large impact parameters,  $p + A \rightarrow p + \gamma + A \rightarrow X + A$  [16], see Fig. 8. These ultraperipheral proton-nucleus collisions open a possibility for studies of hard photon-proton



interactions at extremely high energies and allow one to probe the gluon density in the proton at the values of Bjorken  $x$ , which are a factor of ten smaller (for the same virtuality) than those probed at HERA [30, 31, 32].

In this Section, we estimate the ratio of the jet production in hard coherent proton-heavy nucleus diffraction ( $p + A \rightarrow 2\text{jets} + X + A$ ) to the production of hard jets by the photon-proton interaction, where the photon is coherently produced by the elastically recoiled nucleus,  $p + A \rightarrow p + \gamma + A \rightarrow 2\text{jets} + X + A$ . This corresponds to the situation when the generic final state  $X$  in Fig. 8 contains a hard two-jet component and a soft remaining part  $X$ .

Qualitatively, we expect that the ratio of the hard dijet production due to these two mechanisms will be rather small because of the following two suppression effects.

First, hard diffractive dijet production is suppressed by the factor discussed in Sect. II. Second, the shapes of the parton distribution in the photon and in the screened nuclear diffractive PDFs are rather different. In the photon case, the dominant contribution to the photon PDFs comes from  $\beta \sim 1$  corresponding to the kinematics where a pair of jets is at the rapidities close to the gap. On the other hand, in the screened nuclear diffractive PDFs at large virtualities, which are relevant for the measurements at the LHC, the main contribution comes from small  $\beta$ , see Fig. 3 of [17].

Using the definition of the suppression factor  $\lambda^j$  (16), the hard coherent proton-nucleus diffractive dijet cross section can be written as [see Eq. (12)]

$$\frac{d^3\sigma^{p+A \rightarrow 2\text{jets}+X+A}}{dx_1 dp_T^2 dx_{\mathcal{P}}} \propto r_h \sum_{\substack{i,j \\ k,l=q,\bar{q},g}} f_{i/p}(x_1, Q_{\text{eff}}^2) \lambda^j(\beta x_{\mathcal{P}}, Q_{\text{eff}}^2) f_{j/N}^{D(3)}(\beta, Q_{\text{eff}}^2, x_{\mathcal{P}}) \overline{\sum} |\mathcal{M}(ij \rightarrow kl)|^2 \frac{1}{1 + \delta_{kl}}, \quad (19)$$

In the second line of Eq. (19), we introduced an additional suppression factor  $r_h$ ,

$$\tilde{f}_{j/N}^{D(3)} = r_h f_{j/N}^{D(3)}, \quad (20)$$

which, according to the discussion in Sect. I, takes into account the significant factorization breaking in hard hadron-hadron diffraction.

In our numerical analysis, we used the following model for the suppression factor  $r_h$

$$r_h = \frac{0.75}{N(s)} = 0.75 \left( \int_{1.5/s}^{0.1} dx_{\mathcal{P}} \int_{-\infty}^0 dt f_{\mathcal{P}/p}(x_{\mathcal{P}}, t) \right)^{-1}. \quad (21)$$

This expression is based on the phenomenological model of [10], which describes the suppression of diffraction at the Tevatron ( $\sqrt{s} = 546$  and  $1800$  GeV) by rescaling the Pomeron flux,  $f_{\mathbb{P}/p}(x_{\mathbb{P}}, t)$ , by the factor  $N(s)$ . In Eq. (21), the Pomeron flux is given by the following expression

$$f_{\mathbb{P}/p}(x_{\mathbb{P}}, t) = \frac{1}{x_{\mathbb{P}}^{1+2\epsilon+2\alpha't}} \frac{\beta_{\mathbb{P}pp}^2(t)}{16\pi}, \quad (22)$$

where  $\epsilon = 0.1$ ;  $\alpha' = 0.25$  GeV $^{-2}$ ;  $\beta_{\mathbb{P}pp}(t)$  is the  $\mathbb{P}pp$  form factor [10].

We also introduced the additional factor 0.75 in Eq. (21) in order to phenomenologically take into account the observation that the effects of factorization breaking should be larger in the elementary diffractive PDFs at  $t = 0$  [see Eq. (16)] than in the  $t$ -integrated diffractive PDFs [see Eq. (21)].

The application of Eq. (21) at the RHIC and LHC energies gives

$$\begin{aligned} r_{\text{h}} &= \frac{1}{4.2}, & \text{RHIC}, \\ r_{\text{h}} &= \frac{1}{16.0}, & \text{LHC}. \end{aligned} \quad (23)$$

Note that as follows from the definition (21), the suppression factor  $r_{\text{h}}$  is assumed to be  $x_{\mathbb{P}}$ -independent.

Next we discuss the hard coherent dijet production in proton-nucleus scattering via the e.m. mechanism, when the nucleus coherently emits a quasi-real photon which interacts with the proton and diffractively produces two hard jets,  $p + A \rightarrow p + \gamma + A \rightarrow 2 \text{ jets} + X + A$ , see Fig. 8. The corresponding cross section can be written as a sum of the resolved and direct photon contributions (the separation into the resolved and direct components is only meaningful in the leading-order calculation)

$$\begin{aligned} \frac{d^3 \sigma_{\text{e.m.}}^{p+A \rightarrow 2 \text{ jets} + X + A}}{dx_1 dp_T^2 dx_{\mathbb{P}}} &\propto r_{\text{e.m.}} \sum_{\substack{i,j, \\ k,l=q,\bar{q},g}} f_{i/p}(x_1, Q_{\text{eff}}^2) \frac{n(x_{\mathbb{P}})}{x_{\mathbb{P}}} f_{j/\gamma}(\beta, Q_{\text{eff}}^2) \overline{\sum} |\mathcal{M}(ij \rightarrow kl)|^2 \frac{1}{1 + \delta_{kl}} \\ &+ \sum_{\substack{i,j, \\ k,l=q,\bar{q},g}} f_{i/p}(x_1, Q_{\text{eff}}^2) \frac{n(x_{\mathbb{P}})}{x_{\mathbb{P}}} \delta(\beta - 1) \overline{\sum} |\mathcal{M}(i\gamma \rightarrow kl)|^2 \frac{1}{1 + \delta_{kl}}, \end{aligned} \quad (24)$$

where  $n(x_{\mathbb{P}})$  is the flux of equivalent photons [30] expressed in terms of  $x_{\mathbb{P}}$  instead of the photon energy  $\omega$  (note the factor  $1/x_{\mathbb{P}}$  coming from the  $1/\omega$  in the spectrum of the equivalent photons);  $f_{j/\gamma}$  is the PDF of the real photon;  $\overline{\sum} |\mathcal{M}(i\gamma \rightarrow kl)|^2$  are invariant matrix elements for the direct photon-parton scattering, see Table 7.9 in [26];  $r_{\text{e.m.}}$  is a phenomenological

factor describing the factorization breaking for the resolved (hadron-like) component of the real photon. The exact value of  $r_{\text{e.m.}}$  is uncertain: It ranges from  $r_{\text{e.m.}} = 0.34$  [33] to  $r_{\text{e.m.}} \approx 1$  with large errors [34]. Since our analysis is a simple leading-order estimate, we conservatively take  $r_{\text{e.m.}} = 0.5$ .

The flux of equivalent photons approximately equals [30]

$$n(x_{\mathcal{P}}) \approx \frac{2Z^2\alpha_{\text{e.m.}}}{\pi} \ln\left(\frac{\gamma}{R_A x_{\mathcal{P}} p_{\text{lab}}}\right), \quad (25)$$

where  $Z$  is the nuclear charge;  $\gamma$  is the Lorentz factor ( $\gamma \approx 3000$  for  $pPb$  scattering at the LHC [29]);  $R_A = 1.145 A^{1/3}$  fm is the effective nuclear radius;  $p_{\text{lab}}$  is the momentum of the nucleus in the laboratory frame ( $p_{\text{lab}} \approx 2.75$  TeV for  $pPb$  scattering at the LHC). In practice, we used a more precise formula for the flux of the equivalent photons, which reduces the result of Eq. (25) by 11% [35].

We are now ready to estimate the ratio of the hard diffractive dijet cross sections corresponding to the hard and e.m. mechanisms,  $R$ ,

$$R(\beta, x_{\mathcal{P}}, p_T) = \frac{d^3\sigma^{p+A \rightarrow 2\text{jets}+X+A}}{dx_1 dp_T^2 dx_{\mathcal{P}}} \bigg/ \frac{d^3\sigma_{\text{e.m.}}^{p+A \rightarrow 2\text{jets}+X+A}}{dx_1 dp_T^2 dx_{\mathcal{P}}}, \quad (26)$$

where the involved cross section are given by Eqs. (12) and (24) with the equal coefficients of proportionality. In the simplified kinematics that we use, at given  $p_T$  and  $x_{\mathcal{P}}$ , the ratio  $R$  depends only on  $\beta$ .

We considered two cases: The dijet production summed over gluon and quark jets and the production of two heavy-quark jets ( $c$  and  $b$  quarks). The resulting ratios  $R$  at  $p_T = 5$  GeV and  $x_{\mathcal{P}} = 10^{-4}$ ,  $10^{-3}$  and  $10^{-2}$  as functions of  $\beta$  are presented in Fig. 9. The left panel corresponds to quark and gluon jets; the right panel corresponds to heavy-quark jets.

The results presented in Fig. 9 deserve a detailed discussion. The dependence of the ratio  $R$  on  $x_{\mathcal{P}}$  is not too strong and can be explained as follows. The main contribution to the  $x_{\mathcal{P}}$ -dependence of  $R$  at fixed  $\beta$  comes from the changing of  $x_1$ . As  $x_{\mathcal{P}}$  is decreased,  $x_1$  is increased, which diminishes the role played by the gluons in the projectile. As explained in the following, it is the gluon contribution that increases  $R$ . Hence,  $R$  decreases with decreasing  $x_{\mathcal{P}}$ . Note that the dependence of diffractive PDFs on  $x_{\mathcal{P}}$ ,  $f_{j/N}^{D(3)}(\beta, x_{\mathcal{P}}, Q_{\text{eff}}^2) \propto 1/x_{\mathcal{P}}^{1+2\epsilon}$ , see Eq. (22), is similar to the  $1/x_{\mathcal{P}} \ln(1/x_{\mathcal{P}})$ -behavior of the e.m. cross section. Therefore, these two factors weakly affect the  $x_{\mathcal{P}}$ -dependence of  $R$ .

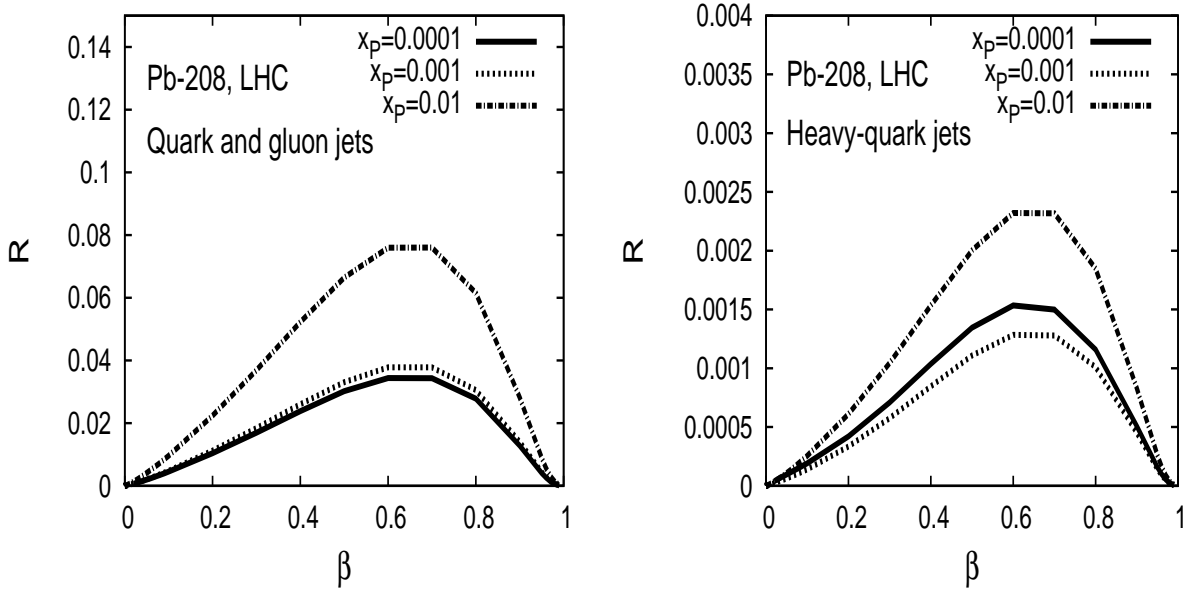


FIG. 9: The suppression of hard diffractive dijet (quark and gluon jets) production compared to e.m. coherent dijet production in proton-Pb scattering at the LHC. The suppression factor  $R$  of Eq. (26) at  $p_T = 5$  GeV and  $x_P = 10^{-4}$ ,  $10^{-3}$  and  $10^{-2}$  as a function of  $\beta$ . The left panel corresponds to quark and gluon jets; the right panel corresponds to heavy-quark jets.

The dependence of  $R$  on  $\beta$  is much faster and reflects different shapes of the proton diffractive PDFs and PDFs of the real photon. While the proton diffractive PDFs times  $\beta$  are flat in the  $\beta \rightarrow 0$  limit, the photon PDFs times  $\beta$  grow. This explains why  $R$  approaches zero when  $\beta$  is small. In the opposite limit,  $\beta \rightarrow 1$ , diffractive PDFs vanish and the e.m. contribution wins over due to the non-vanishing direct photon contribution:  $R \rightarrow 0$  as  $\beta \rightarrow 1$ .

In Fig. 9, the ratio  $R$  at its peak is much larger for the production of quark and gluon jets than for the production of heavy-quark jets. An examination shows that this effect is due to the large gluon diffractive PDF, which in tandem with the large  $gg \rightarrow gg$  hard parton invariant matrix element [26], works to increase  $R$  in the presence of the gluon jets.

We used the following input in our numerical analysis of the ratio  $R$ . We used the LO parameterization of the real photon PDFs from Ref. [36]. We have also checked that the use of a different parameterization [37] leads to rather similar predictions.

For the nucleon diffractive PDFs, we used the recent QCD fit to the H1 data on hard

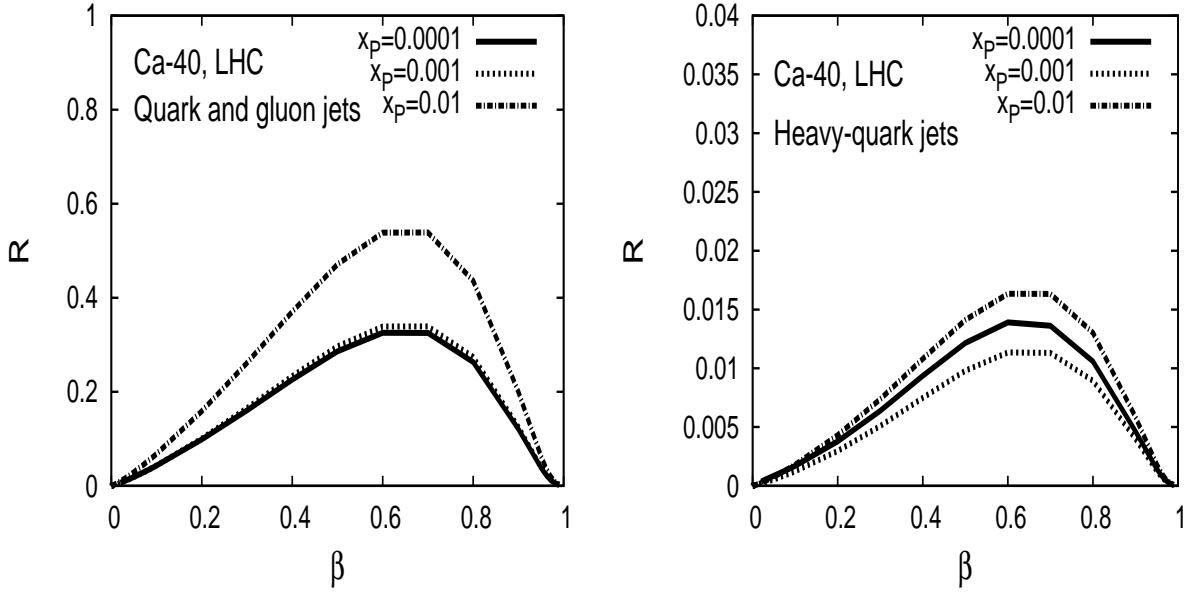


FIG. 10: The suppression factor  $R$  of Eq. (26) for proton- $^{40}\text{Ca}$  scattering at the LHC. The labeling of the curves is the same as in Fig. 9.

inclusive diffraction in DIS on hydrogen [8, 9]. The suppression factor  $\lambda^j$ , which enters Eq. (26) at the scale  $Q^2 = Q_{\text{eff}}^2 = 4p_T^2 = 100 \text{ GeV}^2$ , was evaluated using Eq. (16) with  $\sigma_{\text{eff}}^j(x, Q^2)$  at the same  $Q^2 = Q_{\text{eff}}^2 = 100 \text{ GeV}^2$  scale, see Eq. (7).

The  $\delta$ -function for the direct photon contribution was numerically modeled in the following simple form

$$\delta(\beta - 1) = \frac{1}{\pi} \frac{\epsilon}{(\beta - 1)^2 + \epsilon^2}, \quad \text{with } \epsilon = 0.01. \quad (27)$$

It is instructive to examine how our predictions for the suppression factor  $R$  change, when the heavy nucleus of  $^{208}\text{Pb}$  is replaced by a lighter nucleus of  $^{40}\text{Ca}$ . Note that for  $pCa$  scattering at the LHC,  $\sqrt{s} = 9.9 \text{ TeV}$  and  $\gamma \approx 3700$  [29]. We expect that the ratio  $R$  will significantly increase because of the reduction of the flux of the equivalent photons [the flux is proportional  $Z^2$  (25)].

Figure 10 presents the ratio  $R$  for  $^{40}\text{Ca}$ . The labeling of the curves is the same as in Fig. 9. As can be seen from the comparison of Figs. 10 and 9, the ratio  $R$  increases by the factor  $\approx 7 - 10$ , when going from  $^{208}\text{Pb}$  to  $^{40}\text{Ca}$ .

Besides the LHC, RHIC also has a potential to measure hard diffraction in proton-nucleus scattering. We consider a typical example of the corresponding RHIC kinematics with 250 GeV protons scattering on 100 GeV/per nucleon nuclei (the corresponding  $\sqrt{s} \approx 320 \text{ GeV}$

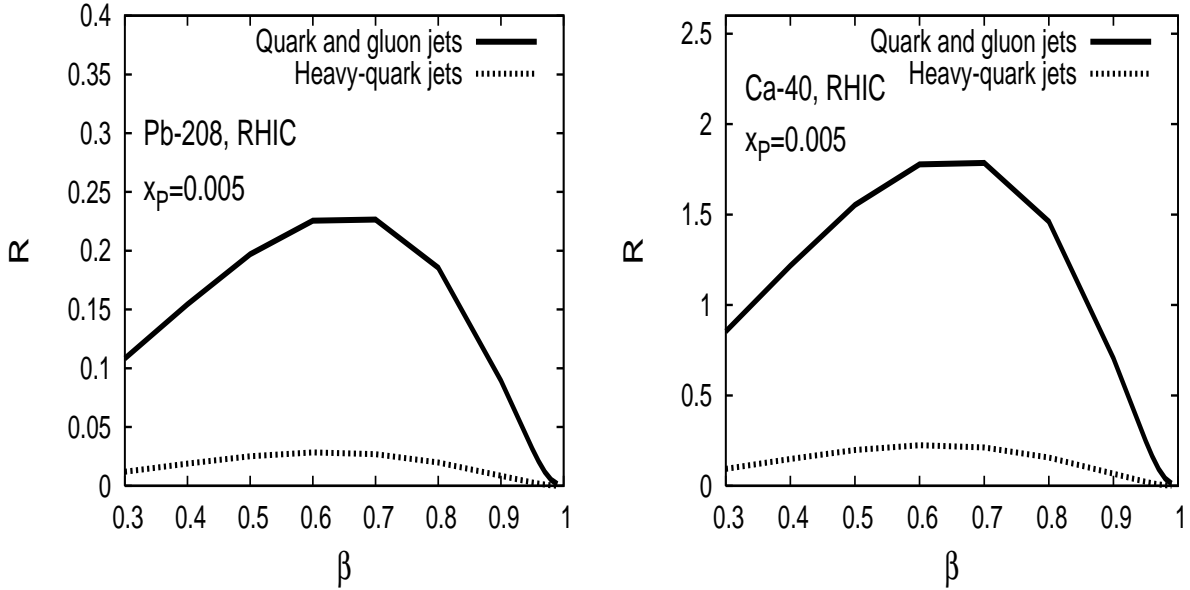


FIG. 11: The suppression factor  $R$  of Eq. (26) in the RHIC kinematics and at  $p_T = 5$  GeV and  $x_P = 5 \times 10^{-3}$  as a function of  $\beta$ . The solid curves correspond to quark and gluon jets; the dotted curves correspond to heavy-quark jets.

and the Lorentz dilation factor is  $\gamma \approx 100$ ). Producing sufficiently high diffractive masses, e.g.  $M_X^2 = 500 \text{ GeV}^2$ , one accesses the typical kinematics of hard diffraction,  $x_P = 5 \times 10^{-3}$  and  $\beta > 0.3$ . Note also that the suppression of hard diffraction at RHIC is approximately four times smaller than at the LHC, see Eq. (23).

We studied the suppression factor  $R$  of Eq. (26) in the considered RHIC kinematics at  $p_T = 5$  GeV. The resulting values of  $R$  as a function of  $\beta$  are presented in Fig. 11. The solid curves correspond to quark and gluon jets; the dotted curves correspond to heavy-quark jets.

As seen from Fig. 11, the factor  $R$  at RHIC is larger than at the LHC. This is mostly a consequence of the decrease of the flux of equivalent photons when going from the LHC to the RHIC kinematics.

#### IV. CONCLUSIONS

Using the Glauber-Gribov multiple scattering formalism and the leading twist theory of nuclear shadowing, we developed a method for the calculation of coherent hard diffraction

processes off nuclei. We showed that soft multiple rescatterings lead to the factorization breaking of hard diffraction in proton-nucleus scattering, which is larger than the well-known factorization breaking of diffraction in hadron-nucleon scattering.

Based on these results, we compare the hard diffractive to e.m. mechanisms of hard coherent production of two jets in proton-nucleus scattering. We study the  $x_{\mathcal{P}}$ ,  $\beta$  and  $A$ -dependence of the ratio of the dijet production cross sections due to the two effects,  $R$ , at the LHC and RHIC kinematics. We separately study the case when the final jets consist of quarks and gluons and the case when the final jets consist of heavy ( $c$  and  $b$ ) quarks.

Our results can be summarized as follows. For proton- $^{208}\text{Pb}$  scattering at the LHC, hard diffraction is suppressed compared to the e.m. contribution, especially at  $x_{\mathcal{P}} = 10^{-4}$  and large  $\beta$ , e.g.  $\beta > 0.8$ , see Fig. 9. The suppression is very strong for the production of heavy-quark jets, see the right panel of Fig. 9. The physical reason of the suppression is the strong coherent Coulomb field of  $^{208}\text{Pb}$ , which enhances the e.m. mechanism of hard diffraction.

Replacing  $^{208}\text{Pb}$  by  $^{40}\text{Ca}$ , the hard diffractive mechanism becomes compatible to the e.m. one in the case of the production of quark and gluons jets, see the left panel of Fig. 10. However, like in the case of  $^{208}\text{Pb}$ , the production of heavy-quark jets is dominated by the e.m. mechanism, see the right panel of Fig. 10.

As a result of the smaller Lorentz dilation factor  $\gamma$  at RHIC, the factor  $R$  at the RHIC kinematics is larger than at the LHC.

Our results suggest the following experimental strategies. First, the use of heavy nuclei in  $pA$  scattering at the LHC will provide a clean method to study hard real photon-proton scattering at the energies exceeding the HERA energies by the factor of ten. Second, taking lighter nuclei and choosing the appropriate kinematics, where the e.m. contribution can be controlled, one can effectively study the factorization breaking in nuclear diffractive PDFs. Third, in the same kinematics, a comparison of the dijet diffractive production to the heavy-quark-jet diffractive production will measure the nuclear screened diffractive gluon PDF. It can be compared to the nuclear diffractive PDFs, which will be measured in nucleus-nucleus ultraperipheral collisions at the LHC.

## Acknowledgments

We would like to thank K. Goulianos for valuable discussions of the factorization breaking in  $p\bar{p}$  diffraction and M. Zhalov for the discussions of the suppression factor for hard diffraction and the calculation of the correction to the flux of equivalent photons. This work is supported by the Sofia Kovalevskaya Program of the Alexander von Humboldt Foundation (Germany) and DOE (USA). M.S. thanks the Frankfurt Institute for Advanced Studies at Frankfurt University for the hospitality during the time when this work was completed.

- 
- [1] R. Bonino *et al.* [UA8 Collaboration], Phys. Lett. B **211** (1988) 239.
  - [2] K. Goulianos, arXiv:hep-ph/0407035.
  - [3] H. Abramowicz and A. Caldwell, Rev. Mod. Phys. **71** (1999) 1275 [arXiv:hep-ex/9903037].
  - [4] J. C. Collins, Phys. Rev. D **57** (1998) 3051 [Erratum-ibid. D **61** (2000) 019902] [arXiv:hep-ph/9709499].
  - [5] J. Breitweg *et al.* [ZEUS Collaboration], Eur. Phys. J. C **6** (1999) 43 [arXiv:hep-ex/9807010].
  - [6] C. Adloff *et al.* [H1 Collaboration], Z. Phys. C **76** (1997) 613 [arXiv:hep-ex/9708016].
  - [7] C. Adloff *et al.* [H1 Collaboration], Eur. Phys. J. C **20** (2001) 29 [arXiv:hep-ex/0012051].
  - [8] [H1 Collaboration], arXiv:hep-ex/0606004.
  - [9] [H1 Collaboration], arXiv:hep-ex/0606003.
  - [10] K. Goulianos, Phys. Lett. B **358** (1995) 379.
  - [11] A. B. Kaidalov, V. A. Khoze, A. D. Martin and M. G. Ryskin, Eur. Phys. J. C **21** (2001) 521 [arXiv:hep-ph/0105145].
  - [12] L. Frankfurt, M. Strikman, C. Weiss and M. Zhalov, Czech. J. Phys. **55** (2005) B675 [arXiv:hep-ph/0412260].
  - [13] L. Frankfurt, G. A. Miller and M. Strikman, Phys. Rev. Lett. **71** (1993) 2859 [arXiv:hep-ph/9309285].
  - [14] M. Strikman and V. Guzey, Phys. Rev. C **52** (1995) 1189 [arXiv:nucl-th/9506010].
  - [15] L. Frankfurt, V. Guzey and M. Strikman, J. Phys. G **27** (2001) R23 [arXiv:hep-ph/0010248].
  - [16] V. Guzey and M. Strikman, Phys. Lett. B **633** (2006) 245 [arXiv:hep-ph/0505088].
  - [17] L. Frankfurt, V. Guzey and M. Strikman, Phys. Lett. B **586** (2004) 41 [arXiv:hep-ph/0308189].



- [18] L. Frankfurt, V. Guzey and M. Strikman, Phys. Rev. D **71** (2005) 054001 [arXiv:hep-ph/0303022].
- [19] R. J. Glauber, Phys. Rev. **100** (1955) 242.
- [20] R. J. Glauber and G. Matthiae, Nucl. Phys. B **21** (1970) 135.
- [21] V. N. Gribov, Sov. Phys. JETP **29** (1969) 483 [Zh. Eksp. Teor. Fiz. **56** (1969) 892].
- [22] E.L. Feinberg and I.Ia. Pomerancuk, Suppl. Nuovo Cimento **III**, 652 (1956).
- [23] M.L. Good and W.D. Walker, Phys. Rev. **120**, 1857 (1960).
- [24] L. Frankfurt and M. Strikman, Eur. Phys. J. A **5** (1999) 293 [arXiv:hep-ph/9812322].
- [25] H. L. Lai *et al.* [CTEQ Collaboration], Eur. Phys. J. C **12** (2000) 375 [arXiv:hep-ph/9903282].
- [26] R.K. Ellis, W.J. Stirling and B.R. Webber, *QCD and Collider Physics*, Cambridge Univ. Press, 1996, p. 248.
- [27] A. Donnachie and P. V. Landshoff, Phys. Lett. B **296** (1992) 227 [arXiv:hep-ph/9209205].
- [28] C. W. De Jager, H. De Vries and C. De Vries, Atom. Data Nucl. Data Tabl. **36** (1987) 495.
- [29] A. Morsch, in *Hard probes in heavy-ion collisions at the LHC*, Eds. M. Mangano, H. Satz and U. Wiedemann, report CERN-2004-009, CERN, 2004.
- [30] G. Baur, K. Hencken, D. Trautmann, S. Sadovsky and Y. Kharlov, Phys. Rept. **364** (2002) 359 [arXiv:hep-ph/0112211].
- [31] C. A. Bertulani, S. R. Klein and J. Nystrand, Ann. Rev. Nucl. Part. Sci. **55** (2005) 271 [arXiv:nucl-ex/0502005].
- [32] M. Strikman, R. Vogt and S. White, Phys. Rev. Lett. **96** (2006) 082001 [arXiv:hep-ph/0508296].
- [33] M. Klasen and G. Kramer, Phys. Rev. Lett. **93** (2004) 232002 [arXiv:hep-ph/0410105].
- [34] S. Chekanov *et al.* [ZEUS Collaboration], Eur. Phys. J. C **23** (2002) 615 [arXiv:hep-ex/0112029].
- [35] M. Zhalov, private communication.
- [36] M. Gluck, E. Reya and A. Vogt, Phys. Rev. D **46** (1992) 1973.
- [37] H. Abramowicz, K. Charchula and A. Levy, Phys. Lett. B **269** (1991) 458.